Investigation of the thermal processes in electron-beam surface modification by means of a scanning electron beam

M Ormanova[1,3], Vl Angelov[2] and P Petrov[1]

[1]Emil Djakov Institute of Electronics, Bulgarian Academy of Sciences,
72 Tzarigradsko Chaussee, 1784 Sofia, Bulgaria
[2]Institute for Nuclear Research and Nuclear Energy, Bulgarian Academy of Sciences,
72 Tzarigradsko Chaussee, 1784 Sofia, Bulgaria

E-mail: maria_mecheva@abv.bg

Abstract. In this work we present a study of the thermal processes taking place during surface modification of steels performed by a scanning electron beam. The model is based on solving the heat transfer equation by means of Green functions. The thermal field was calculated, together with the size of the zone of structural changes in tool steel samples. The comparison of the zones of thermal treatment as experimentally obtained and theoretically calculated and the corresponding structural changes show a very good agreement.

1. Introduction

The use of high-intensity electron beams for modification of metals and alloys leads to enhancement of the techniques for improvement of their physical and mechanical properties.

When a beam of fast electrons interacts with the metal surface, the electron's kinetic energy is transformed into heat, which spreads from the surface to the inner core of the metallic sample. The rates of heating and cooling with this processing method are significantly higher as compared to the oven heating and bath cooling. This leads to specifics in the phase and structural transitions of the metals and their alloys [1-3].

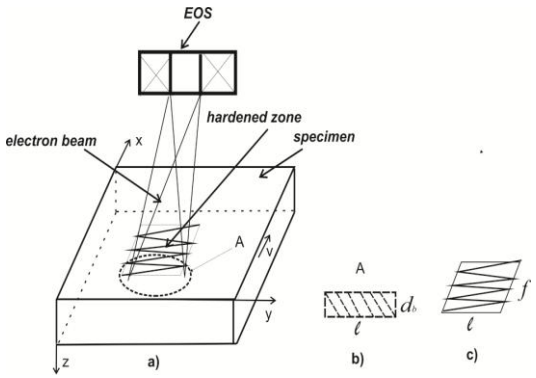

Figure 1. Schematic diagram of a scanning electron-beam treatment setup.

Experimental and numerical methods are used for determination of the temperature field, and thus, of the heating and cooling rates, the final micro-structure and the mechanical properties of the processed samples. The experimental methods are extremely time- and effort-consuming and the obtained results are not always reliable [4,5]. Therefore, the numerical methods are more promising and are widely used for modelling the thermal processes described above [6]. Works [7,8] present results from the investigation of the thermal field distribution

[3] To whom any correspondence should be addressed.

during processing of steels by means of a scanning electron beam (figure 1a). The method of finite elements has been used for solving the equation of heat transfer, with the assumption that the electron beam energy is evenly distributed over a rectangular with area $S = d_b l$ (figure 1b). Here d_b is the electron beam diameter, l is the beam deviation amplitude. In actual experiments, however, the electron beam scans the sample surface following a certain trajectory, as shown in figure 1c, with given scanning frequency and amplitude.

In this work we present a thermal model, whereby the electron-beam energy distribution is obtained by taking into account the frequency and amplitude of beam scanning over the trajectory according to figure 1c. The model is based on solving the heat transfer equation by means of Green functions. The thermal field and the size of the structural changes zone were calculated for instrumental steel samples.

2. Thermal model

The heat transfer equation is solved by means of Green functions, presented in [9] for the case of high-intensity scanning electron beams. The equation has the form:

$$\frac{1}{\alpha}\frac{\partial T}{\partial t} - \nabla^2 T = \frac{f(r,t)}{\lambda}, \tag{1}$$

where $\alpha = \frac{\lambda}{c\rho}$ is the heat exchange coefficient.

$T(r,t)$ is expressed in terms of the three-dimensional Green's function as follows:

$$T(r,t) = \frac{k}{\lambda}\int_{\tau=0}^{t} dt \int_R G(r,t|r',t) f(r',\tau) dv' + \int_R G(r,t|r',\tau)|_{\tau=0} F(r') dv', \tag{2}$$

where $F(r')$ is the initial temperature distribution.

In orthogonal coordinates, the Green's function has the form:

$$G(x,y,z,t|x',y',z',\tau) = G1(x,t|x',\tau) \times G2(y,t|y',\tau) \times G3(z,t|z',\tau), \tag{3}$$

where each of the Green functions G1, G2 and G3 depends on the type of the region (i.e. finite, semi-infinite, or infinite) and on the boundary conditions. The infinite medium Green function is obtained as:

$$G(x,t|x',\tau) = [4\pi\alpha(t-\tau)]^{-1/2} exp\left(-\frac{(x-x')^2}{4\alpha(t-\tau)}\right) \tag{4}$$

and the semi-infinite medium Green function when the boundary at $z' = 0$ is:

$$G(z,t|z',\tau) = [4\pi\alpha(t-\tau)]^{-1/2} \times \left[exp\left(-\frac{(z-z')^2}{4\alpha(t-\tau)}\right) + exp\left(-\frac{(z+z')^2}{4\alpha(t-\tau)}\right)\right], \tag{5}$$

From equations (4, 5) and equation (3) we obtain:

$$G(x,y,z,t|x',y',z'=0,\tau) = 2[4\pi\alpha(t-\tau)]^{-1.5} \times exp\left(-\frac{(x-x')^2 + (y-y')^2 + z^2}{4\alpha(t-\tau)}\right). \tag{6}$$

Substituting $x' = x - r\cos\theta$, $y' = y - r\sin\theta$ and $G(r,t|r',\tau)$ from equation (6) in equation (2), we obtain the temperature distribution:

$$T(x,y,z,t) = T_0 + \frac{2\alpha}{\lambda}\int_0^t \int_{-\pi}^{\pi} \int_0^{\infty} \left[f(x - r\cos\theta, y - r\sin\theta) \times [4\pi\alpha(t-\tau)]^{-1.5} \times exp\left(-\frac{r^2+z^2}{4\alpha(t-\tau)}\right)\right] r dr d\theta d\tau \quad , \tag{7}$$

where α is the heat exchange coefficient, λ is the heat conduction coefficient, x, y, z are the coordinates of the point of calculating the temperature, t is the time of calculating the temperature, r and θ are the polar coordinates of the points of the integration.

For a dithering beam $f_c(x - r\cos\theta,\ y - r\sin\theta,\ \tau)$ we have:

$$f_c(\xi,\eta,\tau) = \frac{3Q}{\pi r_0^2} exp\left(-3\frac{(\xi-v\tau)^2+\left(\eta-\iota_{max}\ \cos\left(\frac{2\pi\tau}{\tau^*}\right)\right)^2}{r_0^2}\right), \quad (8)$$

where $(\xi = x - r\cos\theta, \eta = y - r\sin\theta)$, Q is the transferred power, r_0 is the characteristic beam radius, v is the speed of specimen motion, ι_{max} is the scanning amplitude, τ^* is the scanning period.

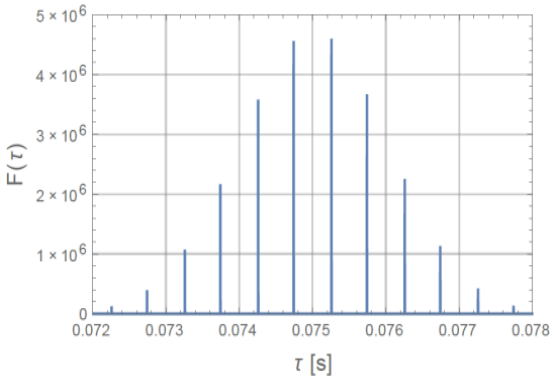

Figure 2. Integrand peaks positions for cosine scanning electron beam along the *x* axis with velocity 40 mm/s, frequency 1 kHz, amplitude 20 mm, beam size 0.1 mm for $\theta = \pi/2$ and r = 1 mm.

The integrand in (7) consists of $2t/\tau^*$ very well separated parts with very small time dimensions and corresponding sharp peaks, as shown in figures 2–4. If the point where we calculate the temperature rise lies on the *x* axis (*y*=0), then the time difference of the peaks for two consecutive integrand parts is $\tau^*/4$.

For the calculations we used the Mathematica numerical integration tool, which works adaptively, reaching a pre-set accuracy. Knowing the exact positions of the integrand parts, the integration was transformed into $2t/\tau^*$ integrations of each integrand part. Finally, the total temperature increase at a given point was calculated as the sum of the contributions of all integrands. Separating the numerical integration into many independent numerical integrations

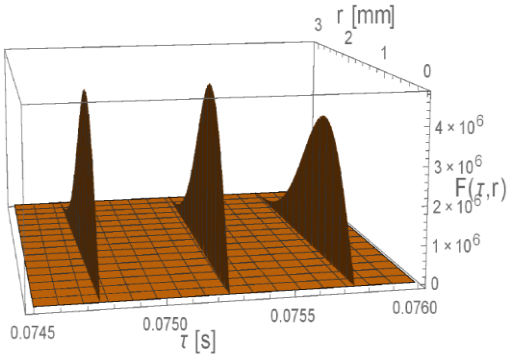

Figure 3. Integrand peaks positions for cosine scanning electron beam along the *x* axis with velocity 40 mm/s, frequency 1 kHz, amplitude 20 mm, beam size 0.1 mm for $\theta = \pi/2$.

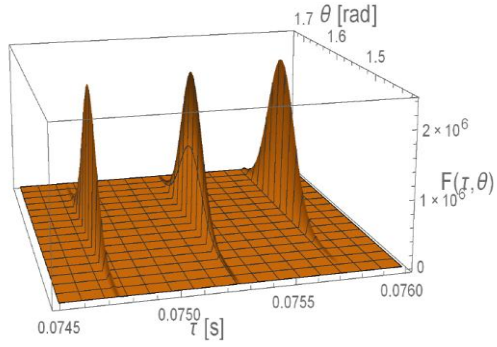

Figure 4. Integrand peaks positions for cosine scanning electron beam along the *x* axis with velocity 40 mm/s, frequency 1 kHz, amplitude 20 mm, beam size 0.1 mm for r = 1 mm.

allows the use of parallel computing implemented in Mathematica for multicore computers, achieving a significant acceleration of the calculation process.

The thermal model used in this work is based on the exact solution of the heat transfer equation by means of the Green functions method and is realized without any approximations. The model is implemented with Mathematica package and all calculations are performed with high accuracy settings. Excellent agreement between results obtained with the Green functions method and the FEM methods results for different cases is reported in [9], which confirms the high reliability of this method.

3. Results and discussion

The numerical calculations of the temperature field were performed according to equations (7,8) with the following technological parameters: accelerating voltage U = 55 kV, electron-beam scanning frequency f = 1 kHz, electron-beam current I = 40 mA, samples motion speed V = 40 mm/s, deviation amplitude l = 20 mm, electron-beam diameter d_l =0,01 mm (q = 2200 W). The specimen was tool steel with the following thermo-physical parameters $\alpha = 7$ mm^2/s, $\lambda = 0.033$ W/mm.K [10, 11].

Figure 5 shows the distribution of the thermal field in the sample depth from z = 0 to z = 1mm, and figure 6, the temperature distribution on the surface, z = 0.

It can be seen that the thermal field is highly inhomogeneous and has a non-stationary nature. The maximal temperature obtained on the surface of the sample (figure 6) is T = 784,625 °C. The calculated value of the treated zone depth (in the temperature interval 500 – 800 °C) is $h_{calc} \approx 100$μm (figure 5). The layers in the sample depth reach a temperature maximum later than the layers close to the surface, the latter having higher heating and cooling rates.

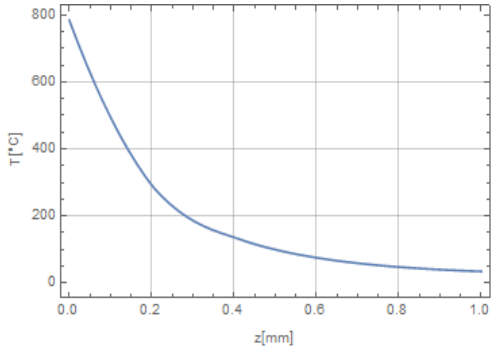

Figure 5. Temperature distribution in depth, from z = 0 to z =1 mm.

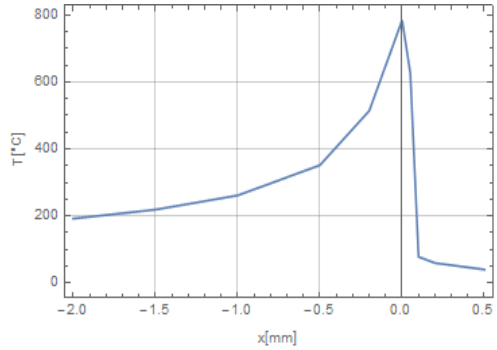

Figure 6. Temperature distribution at the surface, z = 0.

In order to evaluate the applicability of our thermal model, we carried out experiments on samples of tool steel W 320 (0.31% C, 0.30% Si, 0.35% Mn, 2.9% Cr, 2.8% Mo, 0.5% V). Samples with size 20×20×4 mm were subjected to hybrid processing, consisting of preliminary electron-beam hardening (EBH), followed by plasma nitriding (PN) and subsequent electron-beam treatment by means of a scanning electron beam (EBH).

The plasma nitriding was performed under the following technological parameters: T_N = 620 °C; t_N = 24 h; processing gas composition – 70% N_2 + 30% H_2. After plasma nitriding, a layer with a thickness of 10 μm saturated with nitrogen was observed.

The experiments were performed on an electron-beam installation (Leybold Heraus EWS 300/15-60) using a scanning electron beam for the sample processing (figure 1). The technological parameters were the same as those used for the numerical calculations described above.

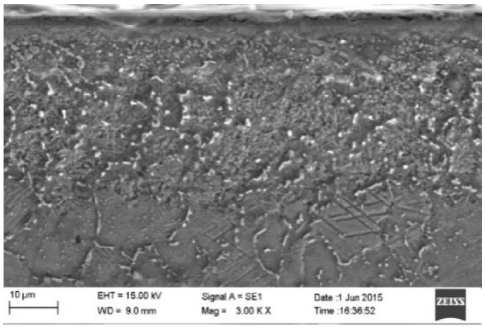

Figure 7. SEM metallographic cross-section after EBH+PN+EBH treatment.

Figure 7 shows a cross-section of the sample after hybrid processing (EBH+PN+EBH). In-depth grain refinement of the sample structure can be seen, which is due to the overlapping (appr. 35÷40 μm) of the plasma nitriding and the subsequent electron beam treatment. In the plasma nitriding, the nitrogen atoms are embedded in the steel crystal lattice, forming nitride phases.

Figure 8 shows the results on the distribution of the hardness in the depth of the treated zone. As a result of the structural changes, the hardness increases up to a distance d=23,76 μm (625,4 kg/mm^2)

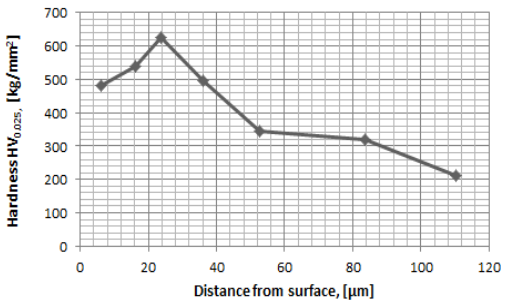

Figure 8. Hardness distribution in depth of the treated zone.

and then gradually decreases. At a distance h_{exp}=110,46 μm, the hardness reaches a value of 210,6 kg/mm^2, which is the hardness of the initial untreated steel. This value can be explained by means of X-ray structural analysis (XRD), which reveals the phases of $FeN_{0.076}$ and Fe_3O_4, having face-centered crystal lattices with lattice parameters a = 0,3626 nm and 0,8379 nm. The presence of $FeN_{0.076}$ in the sample is favorable for the final hardness – it increases by a factor of three.

The comparison of the experimentally obtained (figure 8) and the theoretically calculated (figure 5) treated zone depths shows very good agreement (h_{calc} = 100 μm; h_{exp} = 110,46 μm).

4. Conclusions

A method based on analytical solution of the heat transfer equation by means of Green functions is proposed. The model describes the thermal processes during processing by a scanning electron beam, taking into account the scanning frequency, amplitude and trajectory of the electron beam. The comparison of the experimentally obtained with the theoretically calculated zones of thermal treatment and the corresponding structural changes show a good agreement.

References

[1] Shiller S, Heisig U and Panzer S 1972 *Elektronenstrahltechnologie* (Forschungsinstitut Manfred von Ardene Dresden VEB Verlag Technik) 528
[2] Zenker, R, Sscher G, Buchwalder A, Liebich J, Reiter A and Häßler R 2007 *Surf. Coat. Technol.* **202** 804
[3] Arata Y 1984 *Trans. JWRI* **13** 121 -45
[4] Basile G and Moisan A 1978 *Proc. 2nd Int. Colloq. Welding and Melting by Electron and Laser Beams* (Avignon) 85
[5] Blakeley P 1983 *Proc .3rd Int. Colloq. Welding and Melting by Electron and Laser beams*, (Lyon) 379
[6] Dowden J 2001 *The Mathematics of Thermal Modelling - an Introduction to the Theory of Laser Materials Processing* (Chapman&Hall/CRC) 291
[7] Petrov P and Dimitroff D 1998 *Proc. 6th Int. Conf. Welding and Melting by Electron and Laser Beams* (Toulon) 101
[8] Petrov P 2010 *J. Phys.: Conf. Series* **223** 012029
[9] Farrahi G H and Sistaninia M 2009 *IJE Trans.* A*: Basics* **22**/2 169
[10] Mihailov V, Karhin V and Petrov P 2012 *Fundamentals of Welding* (Tehnika) (In Bulgarian)
[11] Goldak J and Akhlaghi M 2005 *Computational Welding Mechanics* (Springer: USA)